Solar Energy 137 (2016) 551–563

Contents lists available at ScienceDirect

Solar Energy

journal homepage: www.elsevier.com/locate/solener

Six-parameter electrical model for photovoltaic cell/module with compound parabolic concentrator

W. Li [a], M.C. Paul [a,*], N. Sellami [b,c], T. Sweet [d], A. Montecucco [a], J. Siviter [a], H. Baig [b], M. Gao [d], T. Mallick [b], A. Knox [a]

[a] School of Engineering, University of Glasgow, Glasgow G12 8QQ, UK
[b] Environment and Sustainability Institute, University of Exeter, Falmouth Campus, TR10 9FE, UK
[c] School of Engineering & Physical Sciences, Heriot-Watt University, Dubai Campus, PO Box 294345, United Arab Emirates
[d] School of Engineering, Cardiff University, Cardiff CF24 3AA, UK

ARTICLE INFO

Article history:
Received 9 May 2016
Received in revised form 25 August 2016
Accepted 28 August 2016

Keywords:
Photovoltaic cell and module
Compound parabolic concentrator
PV electrical model
Computational fluid dynamics
Multiphysics simulation

ABSTRACT

It is known that compound parabolic concentrators (CPCs) can improve electrical performance of a photovoltaic (PV) flat-plate system. However, a lumped electrical model of a PV cell/module with CPC for assessing performance under different operating conditions is unavailable. In this paper, a six-parameter based model is developed and applied to a PV cell, two PV models with CPC, and a PV module with 2D asymmetric CPC (trough). For validation, CPC with a single PV cell and two CPC modules with 2×2 and 9×9 PV cells are fabricated and measured in an indoor laboratory under standard test conditions. Results show that the optimised algorithm precisely predicts the six model parameters. A sensitivity analysis is performed to identify the importance of each parameter in the model. Ideality factor, circuit current and reverse saturation current are found to be the most dominant factor, while shunt resistance is the least important with CPC gain coefficient and series resistance are in between. Transient performance of a PV cell with CPC under variable outdoor climate conditions is also examined by coupling optical, thermal and electrical effects.

1. Introduction

Current-voltage (I-V) performance curve of a photovoltaic cell/module/panel is critical to their efficient operation under various climate conditions. However, presently I-V curve of a PV cell/module/panel is characterised under standard test conditions (STC, e.g. at 25 °C cell temperature, 1 kW/m^2 irradiance and AM1.5G solar spectrum) in laboratory. In order to obtain an I-V curve and track the maximum electrical output power at the knee of the curve under other operational conditions, a scaling law or method must to be sought. There have been three different approaches to deal with this problem. The first one is a linear interpolation/extrapolation method, in which the I-V curve of target sunlight irradiance and cell temperature is interpolated according to the STC I-V curve and a measured I-V curve under other conditions (Tsuno et al., 2009; Polverini et al., 2011). It is important to note that a series resistance is needed in Polverini et al. (2011) to obtain the I-V curve at a target irradiance and cell temperature. The second one is a five-point translation method, in which the temperature and irradiance are correlated to the current and voltage at five points, namely the short circuit, maximum power, two intermediate and open circuit points. Then the five-point positions can be traced at any target irradiance and cell temperature; finally, an I-V curve can be established with these five points (King et al., 2004). The third one is a lumped model method, in which five (one-diode model) or seven (two-diode model) physical parameters of STC I-V curve are extracted analytically or numerically. The temperature and irradiance are linked to these parameters, and finally, an I-V curve can be established with the updated parameters under a target irradiance and cell temperature. This method is not only simple but also subject to clear physical meanings, so it is increasingly applied in solar energy engineering.

Moreover, there have been three methods for extracting the five or seven lumped physical parameters of a STC I-V curve so far. The first method, such as those proposed by Chan et al. (1986), Villava et al. (2009), Lo Brano et al. (2010, 2012), Carrero et al. (2010, 2011), Zhu et al. (2011), Ma et al. (2014), Boyd et al. (2011), Orioli and Di Gangi (2013), Lo Brano and Ciulla (2013), Dobos (2012) and Ding et al. (2014), is based on the current, voltage and current derivative with respect to the voltage at short circuit, maximum power and open circuit points, usually provided by solar

* Corresponding author.
E-mail address: Manosh.Paul@glagow.ac.uk (M.C. Paul).

http://dx.doi.org/10.1016/j.solener.2016.08.050
0038-092X/

manufactures with product specification sheets. The second method proposed by Siddiqui and Abido (2013) relies on five points that are specified by King et al. (2004) at STC. The third method is a least squares curve fitting technique where a series of I-V points are fitted with the lumped physical electrical model of a PV cell/module/panel by minimising the squared error between predicted and measured currents at all measured voltages to determine five or seven model parameters. To achieve a better curve fitting various optimisation algorithms, namely Newton model in Easwarakhanthan et al. (1986), Levenberg-Marquardt method in Ikegami et al. (2001), genetic algorithms in Zagrouba et al. (2010) and Ismail et al. (2013), pattern search in AlHajri et al. (2012) and AlRashidi et al. (2011), simulated annealing algorithm in El-Naggar et al. (2012), bird mating optimizer in Askarzadeh and Rezazadeh (2013) and improved artificial fish swarm algorithm in Han et al. (2014), have been applied to carry out the minimising procedure. Besides, an analytical approach is proposed to estimate four parameters – ideality, reverse saturation current, series resistance and shunt resistance of PV cell under an irradiance and cell temperature in Kim and Choi (2010). In Wolf and Benda (2013), it is shown that the series resistance can be estimated analytically with two points on the I-V curve near the open circuit point, and the other four parameters are decided by means of a multiple linear regression method.

Compound parabolic concentrators CPC are optical devices applied for solar energy collection. CPCs have experienced an extensive development because they can achieve a high level of concentration to maximise insolation and thus to improve solar cell photon-generated current and power production. The design, optical and thermal property analysis of a CPC can be traced back to 1970s (Winston, 1974; Rabl, 1976). In that time, CPC was considered to be two-dimensional in shape, i.e. a trough. Currently, CPCs can be in three-dimensional shape, namely a polygonal aperture (Cooper et al., 2013). More recently, asymmetric (Baig et al., 2013, 2014) and symmetric (Mammo et al., 2013; Sellami and Mallick, 2013; Baig et al., 2015) CPCs have also found their application in PV cells to increase cell electrical power. However, to the best of our knowledge, there has not been a lumped model available for PV cells/modules/panels with CPC, thus severely restricting the scope of conducting any optical-thermal-electrical multiphysics simulation for CPC optimisation using thermal based CFD software such as ANSYS CFX.

In this article, we develop a six-parameter lumped electrical model for PV cell/modules with CPC and integrate with a 3D heat transfer code, namely ANSYS CFX, to carry out a coupled optical-thermal-electrical multiphysics simulation. Firstly, the six-parameter lumped electrical model for PV cell/module with CPC based on the existing one-diode and five–parameter electrical model with CPC concentration ratio (CR) is presented. Secondly, the optimisation algorithm for the model is verified with an existing ordinary PV cell/module. Thirdly, the model itself is validated against one PV cell and two PV modules measured in our PV indoor laboratory as well as with one PV module found in literature. Then, a sensitivity analysis for the model is carried out to accurately determine the value of the parameters of interest. Finally, the model is integrated into a transient optical-thermal-electrical multiphysics simulation of a PV cell with CPC under an outdoor climate condition.

2. Experimental procedures

Two modules (2×2 and 9×9) of CPC with a concentration ratio, $CR = 3.6$, are designed and fabricated, as shown in Fig. 1 (a) and (b). The profile of the modules is same as that of a single CPC studied in Sellami and Mallick (2013). These CPC modules are assembled with monocrystalline silicon solar (MSS) cells at the aperture of the CPC to form two PV module units for performing indoor experiment. A film with as high as 0.94 reflectance is attached to the CPC's inside surfaces, and a glass cover is glued respectively on top of the CPC and bottom of the PV cells, as shown in Fig. 1(c).

The MSS solar cells used are provided by Solar Capture Technologies, UK, with a laser grooved buried contact for a $CR < 10$. The number of fingers, their thickness and distribution on the solar cell are illustrated in Fig. 1(d). 10 mm $\times$ 10 mm size silicon solar cells are cut from an original silicon wafer with the bus bar and finger patterns, presented in Fig. 1(e).

The PV cells and modules without CPC as well as those with CPC are tested under a solar simulator (WXS-210S-20, AM1.5G, made by Wacom Electric Co. Ltd, Japan), respectively, in the indoor PV laboratory of the Environment and Sustainability Institute, in Falmouth Campus of the University of Exeter to get their STC I-V curves. The simulator has Xenon short arc lamps with unique optical filters to generate an AM1.5G solar spectrum which is subject to ±2% spectral matching and ±0.5% temporal instability. The MP-160 I-V curve tracer made by EKO Instruments is used to measure the I-V curve. A reference solar cell SRC-1000-TC is calibrated under the ISO 17025 VLSI standards and utilised to monitor the irradiance when characterising a solar cell. The simulator usually is warmed up until a steady energy flux achieved for measurement.

Additionally, I-V curves of a single PV unit were measured in School of Engineering, Cardiff University (Sweet et al., 2015). And the third PV module with a dielectric asymmetrical compound parabolic concentrator (ACPC, i.e. a 2D trough) of $CR = 2.82$ was presented in Sarmah et al. (2010). Two small PV modules with 6 silicon solar cells, and two parallel strings with three solar cells in series were constructed with and without ACPC. The solar cells were encapsulated with silicon elastomer (Sylgard-184) and ACPCs were placed on top of the solar cells.

The typical I-V curves of the 2×2 and 9×9 PV modules are illustrated in Fig. 2(a) and (b), respectively. It is observed that the modules with CPC are subject to a much higher current with a slightly larger open circuit voltage compared with those without CPC. The proposed lumped physical model to be presented in the next section will facilitate examination of the effects of this on the module performances.

3. Development and application of the proposed model

It is well-known that a monocrystalline PV cell/module without CPC can be presented by a single diode equivalent circuit with five combined parameters which include photocurrent, I_{ph}, diode reverse saturation current, I_d, diode quality factor i.e. ideality factory, n, combined series resistance, R_s and shunt resistance, R_{sh} (Chan et al., 1986). If these five parameters are known, the I-V curve of a PV cell/module can be established by using the following equation and then the maximum power can be determined (Chan et al., 1986; Villava et al., 2009; Lo Brano et al., 2010, 2012; Carrero et al., 2010, 2011; Zhu et al., 2011; Ma et al., 2014; Boyd et al., 2011; Orioli and Di Gangi, 2013; Lo Brano and Ciulla, 2013; Dobos, 2012; Ding et al., 2014).

$$I = I_{ph} - I_d\left[\exp\left\{\frac{q(V + R_s I)}{nkT}\right\} - 1\right] - \frac{V + R_s I}{R_{sh}} \quad (1)$$

in which V and I are the output voltage and current of a solar cell/module/panel respectively, q is the electron charge and k is the Boltzmann constant.

However, these parameters depend on the PV cell/module material, internal structure and operating condition as well as on both radiation intensity and cell temperature in the silicon layer.

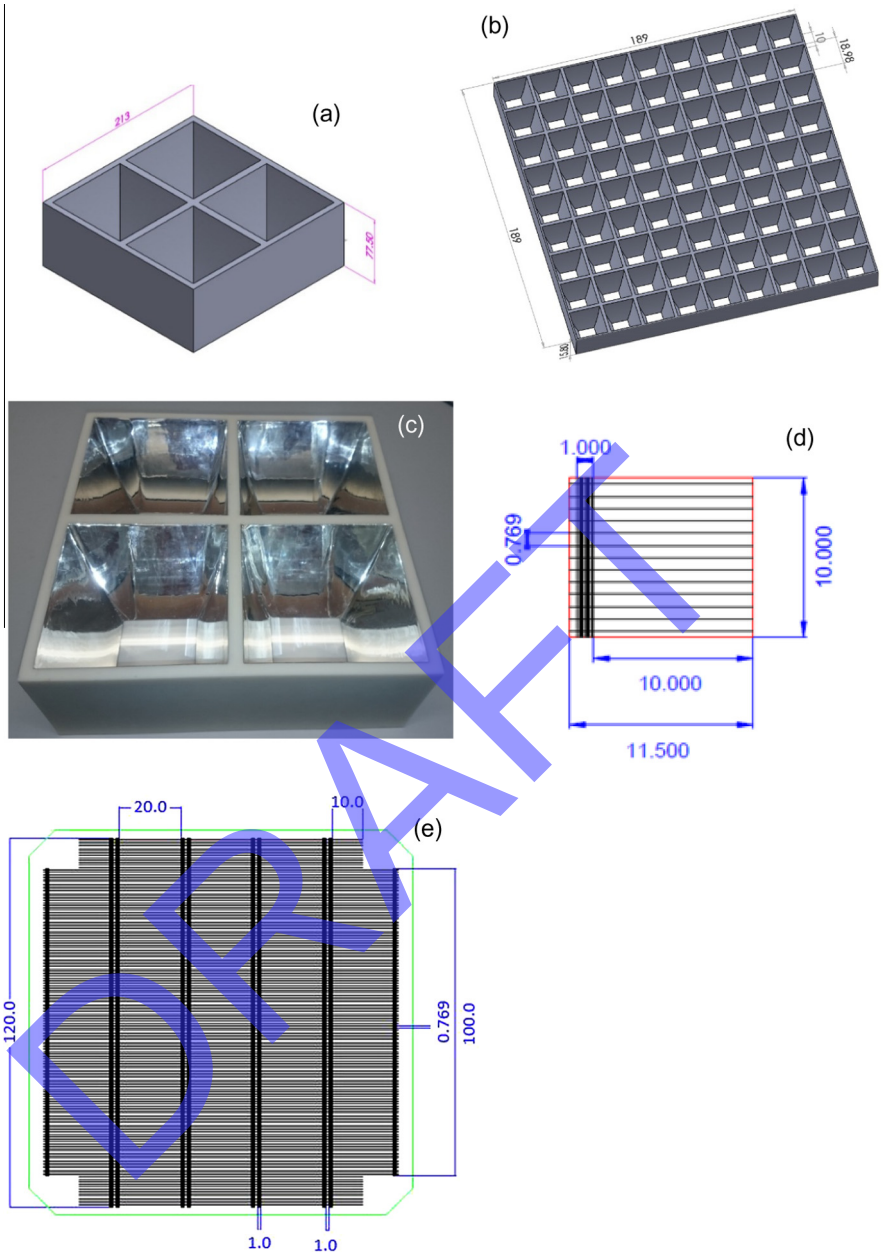

Fig. 1. Profiles of (a) 2 × 2 and (b) 9 × 9 CPC modules, (c) 2 × 2 CPC modules with reflective film of 0.94 reflectance, (d) PV cell with 10 mm × 10 mm size, (e) original silicon wafer.

Determining the value of these parameters is thus key to predict the electrical performance of a PV cell/model. At STC, the photocurrent is equal to the short-circuit current I_{sh0}, and the reverse saturation current, series resistance, ideality factor and shunt resistance are denoted by I_{d0}, R_{s0}, n_0 and R_{sh0}, respectively. Then, Eq. (1) is rewritten as

$$I = I_{sh0} - I_{d0}\left[\exp\left\{\frac{q(V+R_{s0}I)}{n_0 kT_0}\right\} - 1\right] - \frac{V+R_{s0}I}{R_{sh0}} \tag{2}$$

Note that the various mathematical methods mentioned in the introduction have been proposed to extract the five parameters (I_{sh0}, I_{d0}, n_0, R_{s0}, R_{sh0}) at STC from the PV cells/modules without CPC.

To establish the proposed lumped electrical model for the PV cells/modules with CPC, we first look at the experimental I-V curves of the PV cells/modules with and without CPC under the same radiation intensity (1 kW/m^2) at STC (Fig. 2). The photocurrent is more or less doubled, but the open-circuit voltage changes by less than 10%, suggesting the CPC mainly affects the first term in the right-hand side of Eq. (2). A schematic diagram of the model is illustrated in Fig. 3, in which the CPC is considered to be an optical amplifier increasing the sunlight irradiance on the active area of a PV cell/module. Note that the cell temperature is 25 °C in two separate experiments on the I-V curves of the PV cell/module without CPC and with CPC, so the PV cells/modules with CPC share the same I_{d0}, n_0, R_{s0} and R_{sh0}, but a different I_{sh0} with the cells/modules without CPC.

For the mathematical simplicity, we propose that the optical amplifier of CPC to be determined with a gain coefficient, m, so that the photocurrent, as increased by the CPC, is presented in terms of a power function of the concentration ratio and gain coefficient as follows

$$I_{sho,CPC} = CR^m I_{sh0} \tag{3}$$

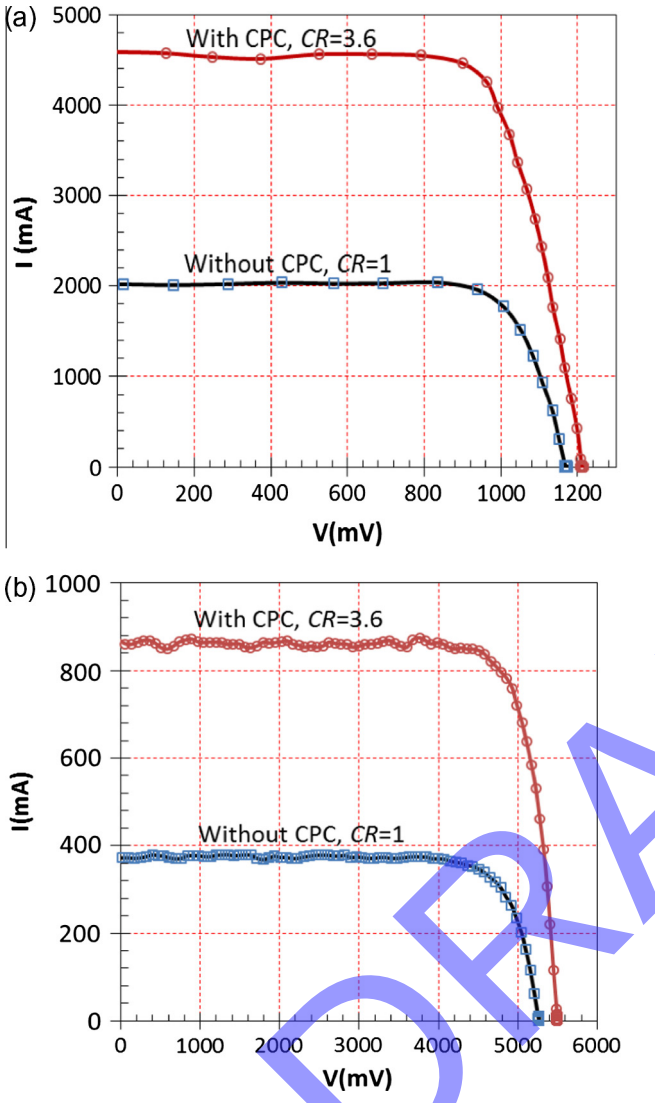

Fig. 2. I-V curves of (a) 2 × 2 and (b) 9 × 9 PV modules with and without CPC at STC.

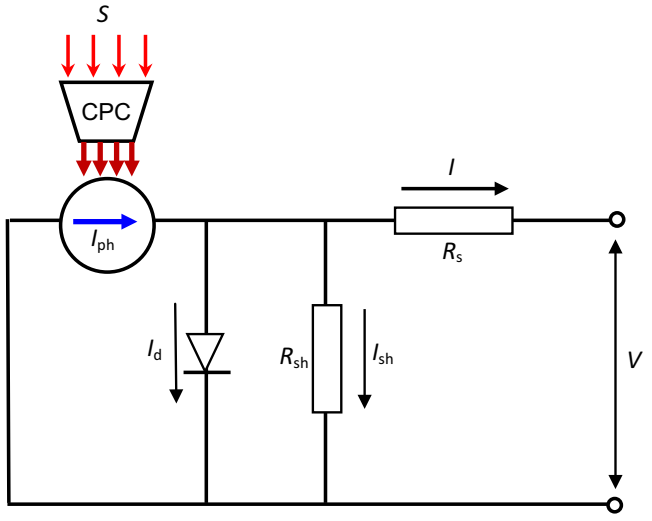

Fig. 3. Schematic of the lumped physical model of I-V curve for the PV cell/module with CPC.

Substituting Eq. (3) into Eq. (2), the I-V curve for the PV cells/modules with CPC at STC is written as

$$I = CR^m I_{sh0} - I_{d0}\left[\exp\left\{\frac{q(V+R_{s0}I)}{n_0 kT_0}\right\} - 1\right] - \frac{V+R_{s0}I}{R_{sh0}} \tag{4}$$

But, for the case without CPC, i.e. implying $CR = 1$, Eq. (4) can restore the case without CPC. Eq. (4) now represents a six-parameter lumped model for a PV cell/module at STC. The six parameters, I_{sh0}, I_{d0}, n_0, R_{s0}, R_{sh0} and m in Eq. (4) are determined based on the experimental I-V curves under two conditions; one for a PV cell/module without CPC, and the other for the same PV cell/module with CPC. The trust-region-reflective (TRR) least squares algorithm provided in MATLAB (2015) is employed to optimise the following objective function for the six parameters

$$f(I_{sh0}, I_{d0}, n_0, R_{s0}, R_{sh0}, m) = \sum_{i=1}^{N_1}(I_{1i} - I_{1i}^{\exp})^2 + \sum_{i=1}^{N_2}(I_{2i} - I_{2i}^{\exp})^2 \rightarrow \min \tag{5}$$

where N_1 and N_2 are the numbers of experimental data of the I-V curves without and with CPC, respectively; I_{1i} and I_{2i} are the currents calculated from Eq. (4) with a set of temporary six parameters at the ith experimental voltages $V_{1i}^{\exp}$ and $V_{2i}^{\exp}$ in the cases without and with CPC, respectively; $I_{1i}^{\exp}$ and $I_{2i}^{\exp}$ are the respective currents at the ith experimental voltages.

Once a set of six parameters are settled, the maximum electrical power is tracked by minimising the following objective function with the same optimisation algorithm as above

$$f(I_{\max}, V_{\max}) = \frac{1}{IV} \rightarrow \min \tag{6}$$

where $I_{\max}$ and $V_{\max}$ respectively are the current and voltage at which a maximum electrical power, $P_{\max}$, is achieved.

3.1. Validation of the algorithm

Initially, the optimisation algorithm is validated against the experimental I-V curves of single PV and module without CPC in Easwarakhanthan et al. (1986). The extracted five parameters and total error, i.e., RMSE (root mean square error) of optimisation defined by the following expression are compared with those obtained by the other nine optimisation algorithms in literature.

$$\varepsilon = \sqrt{\frac{\sum_{i=1}^{N_1}(I_{1i} - I_{1i}^{\exp}) + \sum_{i=1}^{N_2}(I_{2i} - I_{2i}^{\exp})}{N_1 + N_2}} \tag{7}$$

Note that Eq. (7) is for the case where the two experimental I-V curves, i.e. one is for a PV cell or module without CPC and the other one is for a PV cell or module with CPC, are used in the parametric optimisation. When the I-V curve of a PV cell or module without CPC is used in the optimisation process, the second term in the right hand side of Eq. (7) disappears and $N_2 = 0$. Otherwise, i.e. for the I-V curve of a PV cell or module with CPC, the first term from the right hand of Eq. (7) is removed with $N_1 = 0$.

Tables 1 and 2 present these results for the PV cell and PV module respectively. It is seen that the parameters extracted by using the TRR least squares algorithm are similar to those obtained by the others, but with an even smaller error. Only two parameters, such as I_{d0} and R_{sh0}, show some variation across the various algorithms, and overall Tables 1 and 2 demonstrate the TRR algorithm is applicable and suitable for the parameter optimisation for both the PV cells and modules.

Table 1
Comparison of five-model parameters with various methods for PV cell.

Algorithm	R_s (Ω)	R_{sh0} (Ω)	I_{sh0} (A)	I_{d0} (μA)	n	ε	Reference
TRR	0.03634	44.0824	0.7619	0.3004	1.4738	7.4933×10^{-3}	Present
ABSO	0.03659	52.2903	0.7608	0.3062	1.4758	8.0967×10^{-3}	Askarzadeh and Rezazadeh (2013)
BMO	0.03636	53.8716	0.7608	0.3248	1.4817	8.0908×10^{-3}	Askarzadeh and Rezazadeh (2013)
GA	0.0299	42.3729	0.7619	0.8087	1.5751	2.5951×10^{-2}	AlRashidi et al. (2012)
HS	0.03663	53.5946	0.7607	0.3050	1.4754	8.1697×10^{-3}	Askarzadeh and Rezazadeh (2013)
GGSH	0.03631	53.0647	0.7609	0.3262	1.4822	7.9966×10^{-3}	
IGHS	0.03613	53.2845	0.7608	0.3435	1.4874	8.2177×10^{-3}	
PS	0.0313	64.1026	0.7617	0.9980	1.6000	2.5718×10^{-2}	AlHajri et al. (2012)
SA	0.0345	43.1034	0.7620	0.4798	1.5172	2.8118×10^{-2}	Askarzadeh and Rezazadeh (2013)
NLSO	0.0364	53.7634	0.7608	0.3223	1.4837	2.0307×10^{-2}	Easwarakhanthan et al. (1986)

ABSO-artificial bee swarm optimisation, BMO-bird mating optimisation, GA-genetic algorithm, GGHS-groped-based global harmony search, HS-harmony search-based algorithm, IGHS-innovative global harmony search, PS-pattern search, NLSO-nonlinear least-squares optimisation algorithm-Newton model modified with Levenberg parameter, SA-simulated annealing, TRR-trust-region-reflective algorithm in MATLAB.

Table 2
Comparison of five-model parameters with various methods for PV module.

Algorithm	R_s (Ω)	R_{sh0} (Ω)	I_{sh0} (A)	I_{d0} (μA)	n	ε	Reference
TRR	1.0715	590.9428	1.03357	4.9877	50.0294	1.5230×10^{-2}	Present
GA	1.1968	555.5556	1.0441	3.4360	48.5862	4.4988×10^{-2}	AlRashidi et al. (2012)
PS	1.2053	714.2889	1.0313	3.1756	48.2889	4.7547×10^{-2}	AlRashidi et al. (2012)
SA	1.1989	833.3333	1.0331	3.6642	48.8211	1.8835×10^{-2}	Askarzadeh and Rezazadeh (2013)
NLSO	1.2057	549.4505	1.0318	3.2876	48.4500	4.4309×10^{-2}	Easwarakhanthan et al. (1986)

GA-genetic algorithm, PS-pattern search, SA-simulated annealing, NLSO-nonlinear least-squares optimisation algorithm-Newton model modified with Levenberg parameter, SA-simulated annealing, TRR-trust-region-reflective algorithm in MATLAB.

3.2. Extraction of the six parameters

Six parameters of a PV cell and three modules with CPC are determined based on their experimental I-V curves. The I-V curves of the single PV cell with and without CPC were presented in Sweet et al. (2015), while the I-V curves of the two PV modules, namely 2×2 and 9×9 modules, are measured in this work. The single cell and modules share the same CPC profile, as already shown in Fig. 2. The six parameters extracted are tabulated in Table 3 and the I-V curves predicted are compared with the experimental observations in Fig. 4. The predicted I-V curves show good agreement with the measurements for the PV cell and modules with and without CPC. For the PV module with ACPC in Fig. 4(d), however, the agreement is slightly poor, especially when the module is without ACPC in which a solid transparent di-electrical medium is filled (Sarmah et al., 2010). In that case, the PV modules with and without ACPC share the same open-circuit voltage, thus having difficulty in the curve fitting.

Apparently, as seen in Table 3, the six parameters determined are different from the solar cell to module and also reflect with the change in number of solar cells and arrangement. For example, for a CPC, the gain coefficient can be as high as 0.94, but that for an ACPC (2D trough) is just around 0.48, thus showing the former has an excellent optical performance with a resulting good electrical behaviour. In this case, both the I-V curves of the PV cells/modules with and without CPC are utilised in the curve fittings to extract the six parameters. Two additional cases are also investigated based on the I-V curve of a PV cell/module with and without CPC only and the parameters extracted are respectively shown in Tables 4 and 5. Comparison between the results of Tables 3 and 4 demonstrates that the six parameters extracted from the single I-V curve of a PV cell/module with CPC are in reasonable agreement with those from the two I-V curves of the PV cell/module with and without CPC. The five parameters extracted from the single I-V curve of a PV cell/module without CPC in Table 5 are also close to those in Tables 3 and 4. Therefore, this finding confirms that the model proposed here is reasonable since CPCs do not alter the PV cell structure and materials. The radiation intensity may be non-uniformly distributed over the PV cell surface when a CPC is on its top, so there is some difference in values for the parameters extracted from the different I-V curves.

Moreover, the least squares procedure to determine the six parameters in the case, where a single I-V curve of a PV cell with CPC is used, is not robust enough compared with the case with two I-V curves which are fitted simultaneously. Because the number of scattered points in a single I-V curve is nearly less than half of those in the two I-V curves. Thus, it is suggested that in order to obtain a more meaningful set of parameters, two I-V curves of a PV cell/module with and without CPC should be fitted together.

3.3. Sensitivity analysis

A sensitivity analysis is performed to demonstrate the contribution of each parameter to the electrical current or power, and subsequently, they can be ranked from the most important to the least. The most important parameters are determined at the most accuracy, or vice versa. Here the electrical current partial derivatives with respect to the six parameters are derived as follows

Table 3
Parameters extracted from the six-parameter model for the PV cell/module with CPC. The I-V curves of PV cell/module without and with CPC are used simultaneously.

Case	R_{s0} (Ω)	R_{sh0} (Ω)	I_{sh0} (A)	I_{d0} (μA)	n_0	m	ε
Cell	4.3995×10^{-1}	6.3416×10^{3}	2.5718×10^{-2}	1.5248×10^{-5}	1.1042	0.9406	1.6128×10^{-3}
Module (2×2)	1.8921×10^{-2}	1.2925×10^{3}	2.1404	7.7312×10^{-1}	3.0836	0.6011	1.0359×10^{-1}
Module (9×9)	1.1738×10^{-3}	3.0178×10^{3}	3.7717×10^{-1}	3.7721×10^{-1}	10.4431	0.6534	8.5688×10^{-3}
Module (Trough)	3.2530×10^{-1}	6.4844×10^{1}	4.4833×10^{-1}	9.9545	6.4046	0.4777	2.3488×10^{-2}

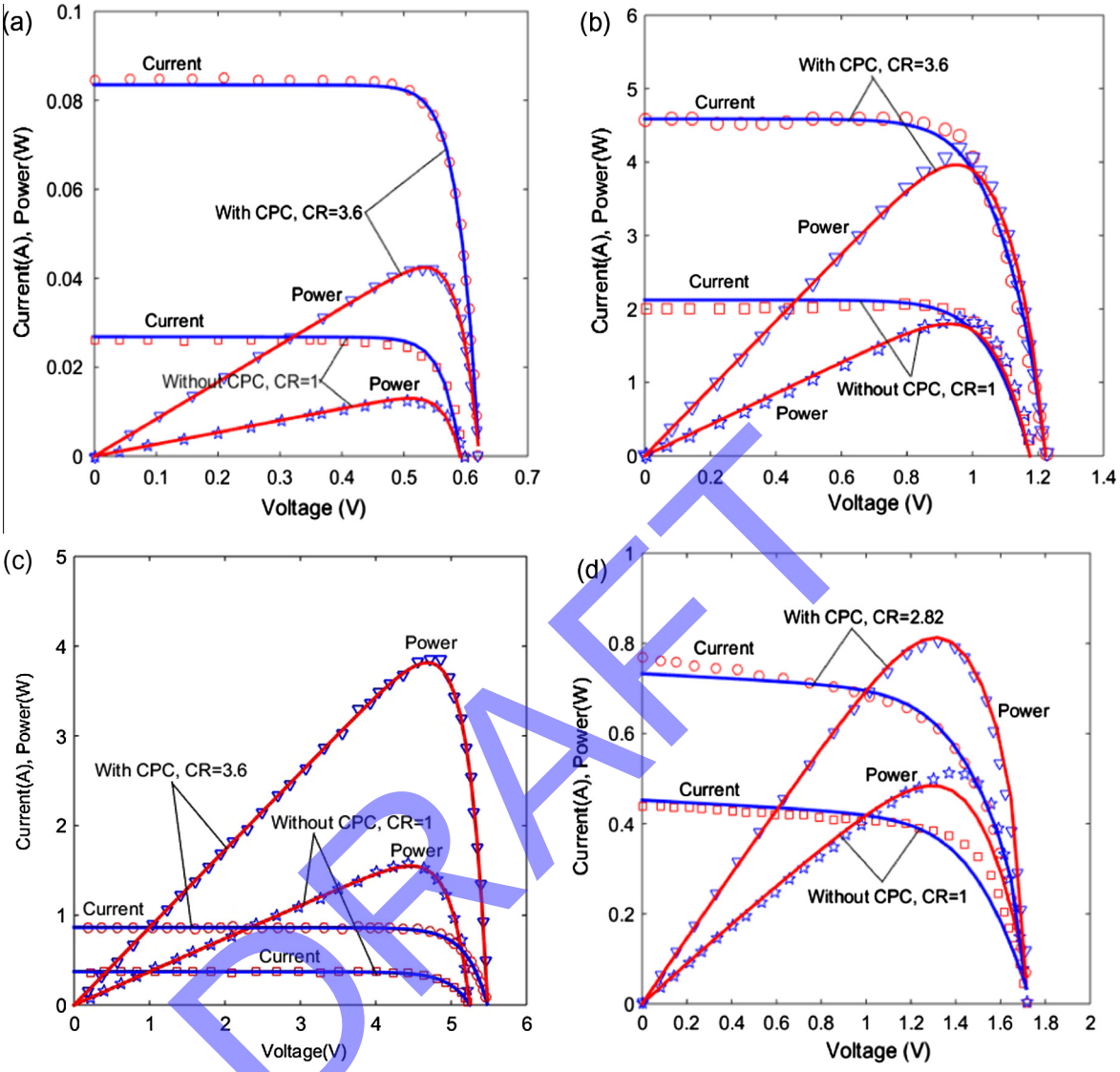

Fig. 4. Comparison of the predicted and tested I-V and P-V curves in four cases, (a) PV cell with CPC, (b) 2 × 2 PV module with CPC, (c) 9 × 9 PV module with CPC, (d) PV module with ACPC. Results of the corresponding systems without CPC for which $CR = 1$ are also shown.

Table 4
Parameters extracted from the six-parameter model for the PV cell/module with CPC. The I-V curve of PV cell/module with CPC is used only.

Case	R_{s0} (Ω)	R_{sh0} (Ω)	I_{sh0} (A)	I_{d0} (μA)	n_0	m	ε
Cell	4.5373×10^{-1}	6.1573×10^{3}	2.8415×10^{-2}	1.6260×10^{-5}	1.1010	0.8611	2.0111×10^{-3}
Module (2 × 2)	1.6300×10^{-2}	1.2925×10^{3}	4.1385	1.3228×10^{0}	3.1642	0.8234	6.7778×10^{-2}
Module (9 × 9)	3.5010×10^{-2}	6.9989×10^{3}	4.4898×10^{-1}	4.7592×10^{-4}	10.0150	0.5099	8.3684×10^{-3}
Module (Trough)	1.0822×10^{-1}	1.3018×10^{1}	5.0247×10^{-1}	5.0469	5.7540	0.4191	2.2237×10^{-3}

Table 5
Parameters extracted from the five-parameter model for the PV cell/module without CPC. The I-V curve of PV cell/module without CPC is used only.

Case	R_{s0} (Ω)	R_{sh0} (Ω)	I_{sh0} (A)	I_{d0} (μA)	n_0	m	ε
Cell	1.2440×10^{-2}	1.3336×10^{3}	2.6105×10^{-2}	2.6105×10^{-5}	1.1835	N/A	2.2956×10^{-4}
Module (2 × 2)	1.4750×10^{-2}	2.5381×10^{4}	2.0365	1.2809×10^{-1}	2.77442	N/A	2.9365×10^{-2}
Module (9 × 9)	1.2540×10^{-2}	1.3719×10^{3}	3.7187×10^{-1}	1.1699×10^{-3}	10.0438	N/A	5.7979×10^{-3}
Module (Trough)	1.0419×10^{-1}	2.8725×10^{1}	4.4312×10^{-1}	4.4312	4.0638	N/A	2.7614×10^{-3}

$$\begin{cases} \partial I/\partial m = mCR^{m-1}I_{sh0} \\ \partial I/\partial I_{sh0} = CR^{m} \\ \partial I/\partial I_{d0} = -\left\{\exp\left[\frac{q(V+R_sI)}{n_0KT_0}\right]-1\right\} \\ \partial I/\partial n_0 = (I_{d0}/n_0)\left[\frac{q(V+R_{s0}I)}{n_0KT_0}\right]\exp\left[\frac{q(V+R_{s0}I)}{n_0KT_0}\right] \\ \partial I/\partial R_{s0} = -\left(\frac{I_{d0}qI}{n_0KT_0}\right)\exp\left[\frac{q(V+R_{s0}I)}{n_0KT_0}\right]-\frac{I}{R_{sh0}} \\ \partial I/\partial R_{sh0} = \frac{VR_{s0}I}{R_{sh0}^2} \end{cases} \quad (8)$$

These partial derivatives for the four cases as shown in Table 3 are calculated in terms of the electrical current after the completion of an optimisation procedure in which the six parameters in Table 3 are imposed to Eq. (8). Then a 10% perturbation is introduced to each parameter to get the six corresponding increments in the electrical current determined by $\Delta I_F = (0.1 \times F)(\partial I/\partial F)$, where F represents a generic parameter. Obviously, if a parameter results in a larger magnitude in the increment, it can have a more important influence on the current and subsequently, will impact the objective function expressed by Eq. (5) more significantly. If a parameter has a greater influence on the objective function, it will be determined more easily and accurately. To evaluate this mathematical property of the six parameters, we rank these from the most important to the least important according to the magnitude of the increment of every parameter. Obviously, the parameter with a higher rank will be decided more precisely in the optimisation process than with a lower rank.

These increments in electrical current of the single PV cell with CPC, the PV modules with 2×2, 9×9 CPC and trough are illustrated as a function of voltage in Fig. 5. The increments due to the change in n_0, I_{sh0} and I_{d0} are larger in magnitude than the increments caused from the rest, thus showing n_0, I_{sh0} and I_{d0} have more important influence upon the electrical current. Based on the absolute magnitude of those increments, the ranking lists in the four cases are shown below from the most to least important,

$$\begin{cases} n_0 > I_{sh0} > I_{d0} > m > R_{s0} > R_{sh0} & \text{single PV cell} \\ n_0 > I_{sh0} > I_{d0} > R_{s0} > m > R_{sh0} & 2 \times 2 \text{ PV module} \\ n_0 > I_{sh0} > I_{d0} > m > R_{s0} > R_{sh0} & 9 \times 9 \text{ PV module} \\ n_0 > I_{sh0} > I_{d0} > R_{s0} > m > R_{sh0} & \text{2D trough PV module} \end{cases} \quad (9)$$

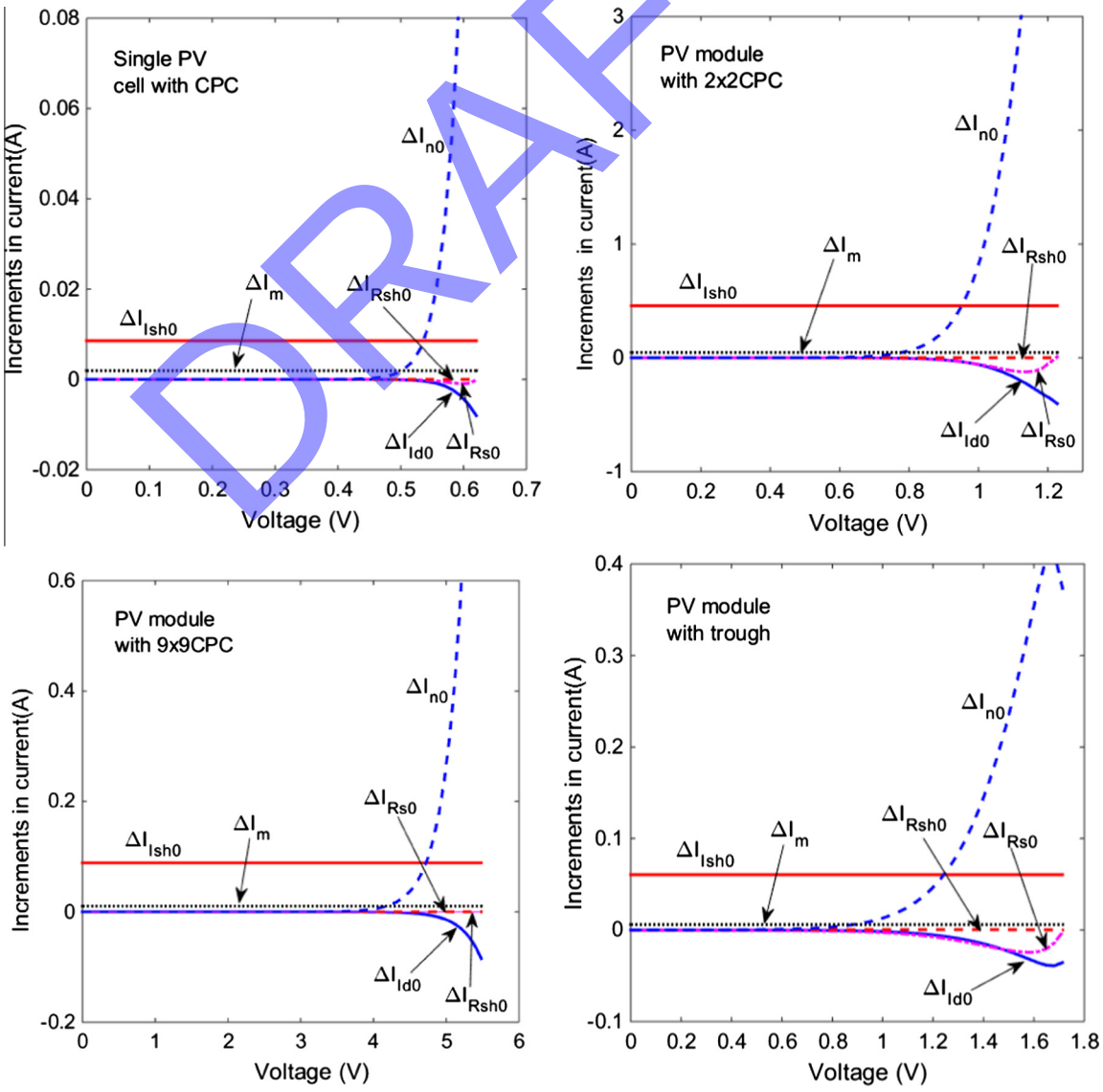

Fig. 5. Increments of electrical current with respect to 10% perturbation in the six parameters presented in Table 3 for the single PV cell, the PV module with 2×2, 9×9 CPC and trough.

Moreover, since n_0, I_{sh0} and I_{d0} make the most dominated contribution to the current, they can be determined with most accuracy. While, R_{sh0} is decided with the least accuracy on account of the tiniest contribution to the current, m and R_{s0} are determined with a reasonable accuracy. Furthermore, it has been observed that R_{sh0} changes least and its value demonstrates having the minimum effect on the current during the optimisation procedure. This thus requires that the initial value of R_{sh0} should be given as close as possible to its true value. Two additional methods are applied to determine this value. Firstly, by conducting a linear regression against 3–5 I-V points near the short circuit point the slope of dI/dV is calculated to obtain $R_{sh0} \approx -\frac{1}{dI/dV}$ (Chan et al., 1986). An average value of the two R_{sh0}, each based on the I-V curves of the cell/module with and without CPC is used as an initial condition for R_{sh0} in the optimisation procedure, determined by

Table 6
The lower and upper limits of six parameters during their optimisation process.

Case	R_{s0} (Ω)	R_{sh0} (Ω)	I_{sh0} (A)	I_{d0} (μA)	n_0	m
Cell	[0, 0.1]	Based on Eq. (10)	[0, 0.1]	$[0, 1 \times 10^{-2}]$	[0, 5]	[0, 1]
Module (2 × 2)	[0, 1]	Based on Eq. (10)	[0, 10]	$[0, 1 \times 10^{3}]$	[0, 10]	[0, 1]
Module (9 × 9)	[0, 10]	Based on Eq. (10)	[0, 1]	$[0, 1 \times 10^{3}]$	[0, 50]	[0, 1]
Module (Trough)	[0, 1]	$[0, R_{sh0}^{max}]$	[0, 1]	$[0, 1 \times 10^{5}]$	[0, 50]	[0, 1]

$R_{sh0}^{max} = R_{s0}^{max} 607.19 \exp(0.1654 I_{sc})$ based on Eq. (11), here R_{s0}^{max} = 1 Ω the PV module with trough.

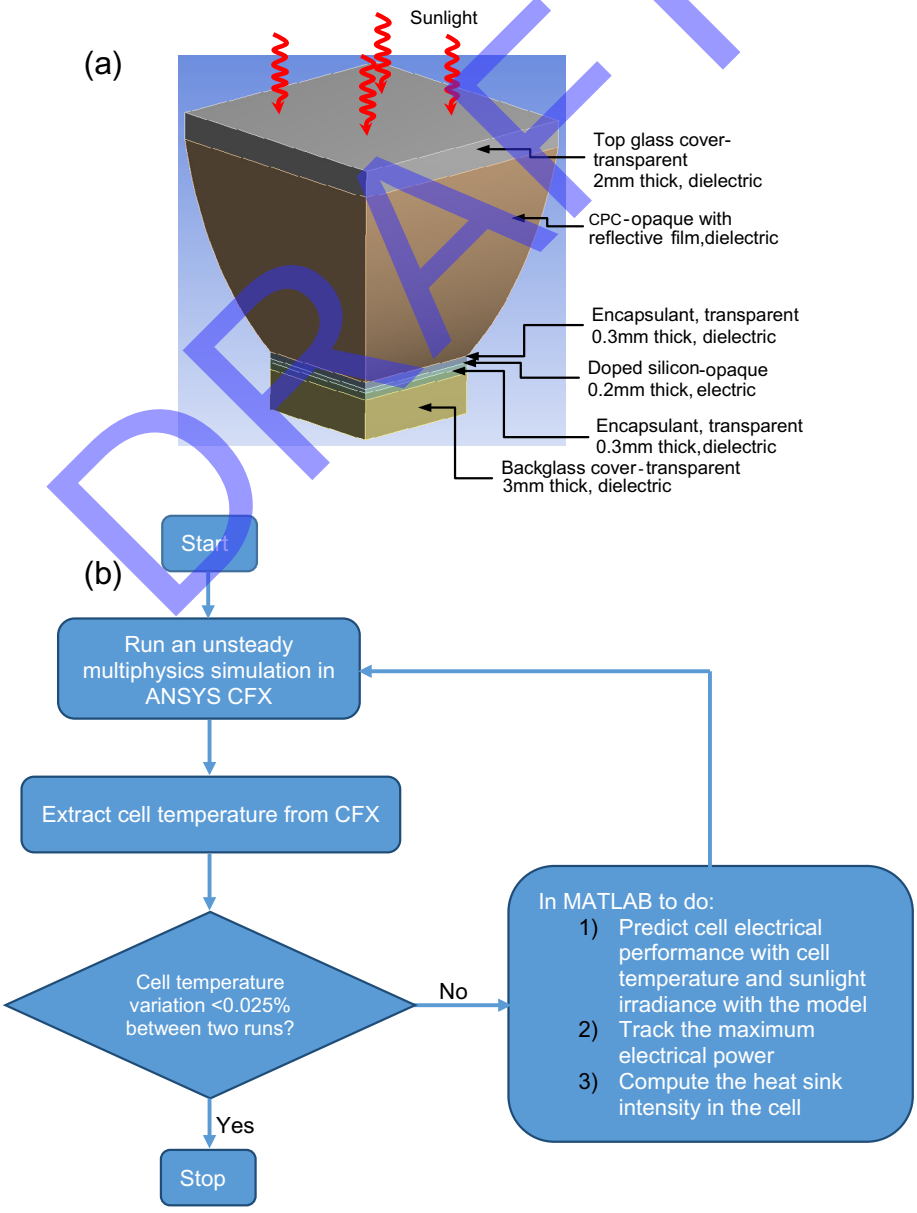

Fig. 6. Components of CPC with solar cell and flowchart of coupling method between CFX solver and lumped I-V curve model in MATLAB, (a) CPC with PV cell, (b) flowchart of coupled method.

$$R_{sh0} \approx \frac{1}{2}\left[\left(-\frac{1}{dI/dV}\right)_{no\ CPC} + \left(-\frac{1}{dI/dV}\right)_{CPC}\right] \quad (10)$$

Secondly, a relationship between R_{sh0} and R_{s0} is established using the following expression and applied in the optimisation procedure. Based on the experimental and calculated results for the PV modules in Ding et al. (2014), we found out that the ratio R_{sh0}/R_{s0} could be correlated to the measured short circuit current I_{sc} as

$$R_{sh0}/R_{s0} = 607.19\exp(0.1654 I_{sc}) \quad (11)$$

Additionally, if the slope of the I-V curves of cell/module with and without CPC is quite different, Eq. (11) should be taken into account. Finally, the lower and upper limits of the six parameters are presented in Table 6 during the optimisation of six parameters.

3.4. Integration of the model with multiphysics analysis

To characterise both the thermal and electrical performances of PV cells or modules with CPC under outdoor condition with variable sunlight radiation intensities, wind speed as well as ambient temperature, it is important to carry out a coupled optical, thermal and electrical simulation. Coupled optical and thermal heat transfer performance of CPC under both steady-state (Li et al., 2015a) and transient (Li et al., 2015b) conditions were previously studied by a CFD method; however, the electrical effect was ignored. Considering an isolated CPC with solar cell, as in Li et al. (2015a, 2015b) and shown in Fig. 6(a), the solar radiation power consumed for generating the electrical power is supposed to be equivalent to the heat sink in the solar cell. The sink intensity is then determined by the maximum electrical power generated by the cell using $s_h = -P_{max}/V_{cell}$, where V_{cell} is the cell volume, and applied to the

Table 7
Optical, radiative and thermal properties of glass, air, sylgard, silicon and reflective film at 25 °C.

Medium	Glass	Air	Sylgard	Silicon	CPC film
Density (kg m^{-3})	2500	1.185	1030	2330	N/A
Specific capacity (J kg^{-1} K^{-1})	750	1004	1100	712	N/A
Thermal conductivity (W m^{-1} K^{-1})	1.4	0.0261	0.16	148	N/A
Absorption coefficient (m^{-1})	2.0	0.01	2.0	70,000	N/A
Scattering coefficient	0	0	0	0	N/A
Refractive index	1.4	1.0	1.42	4	N/A
Emissivity	0.94	0	0.9	0.672	0.06
Diffuse fraction	0	0	0	0	0

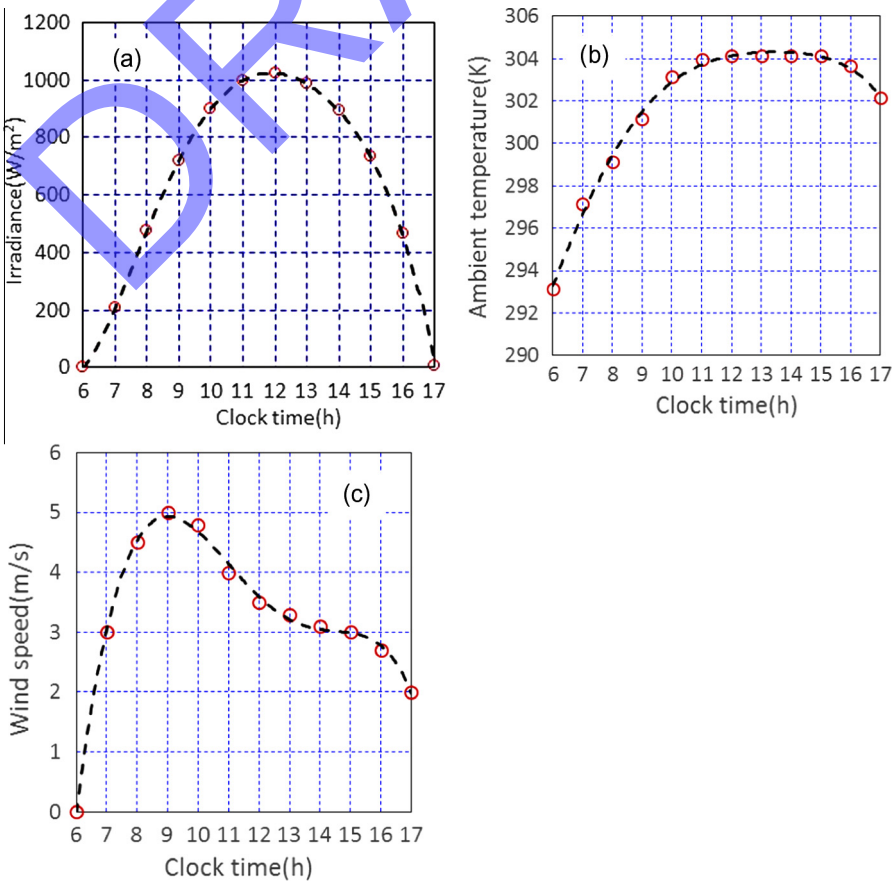

Fig. 7. Monitored solar irradiance, ambient temperature and wind speed in Ortiz-Rivera and Feliciano-Cruz (2009). The dashed lines are for the curve fitting expressed by Eq. (13), and symbols are for the monitored data.

heat transfer equation in the PV cell layer. This thus suggests that the cell/module always works at its maximum power point by making use of a PV tracer. If this is not the case, P_{max} can be replaced with the electrical power at another operating point and the flowchart shown in Fig. 6(b) illustrates this electrical and thermal coupling. However, it is worth noting that the absorbed solar radiation by a flat PV panel, applied to the heat transfer equation as a mechanism to generate an internal heat, is calculated from the panel volume, PV cell efficiency and cell volume (Siddiqui et al., 2012). This method is not used here. Instead, the solar radiation is directly applied to the top glass cover but the electrical power generated is regarded as a heat loss in terms of a negative heat source based on the energy balance point of view. This means that part of the solar energy will be consumed by this source for generating electricity.

The transient performance of CPC with PV cell results from outdoor climate conditions, with ambient temperature, sunlight radiation intensity and wind speed. The electrical lumped model proposed above is applicable only at the STC. To extend the model into a variable outdoor condition, a scaling law for the six parameters is desirable by which the six parameters under outdoor conditions will be determined, and in turn the corresponding I-V curves and the maximum electrical power can be obtained. The well-established two scaling laws for flat-plate PV cells/modules can be found in Dobos (2012), Ikegami et al. (2001), Siddiqui et al. (2012) and De Soto et al. (2006). In those laws, series electrical resistance and ideality remain constant, and photocurrent is related to both the radiation intensity and cell temperature. But the diode reverse saturation current is dependent on the cell temperature, whilst the shunt resistance depends on the radiation intensity only. Combining the scaling laws in Dobos (2012), Siddiqui et al. (2012) and De Soto et al. (2006) and considering the gain coefficient as constant, the following scaling laws are developed

$$\begin{cases} n = n_0 \\ R_s = R_{s0} \\ I_{ph} = CR^m(S/S_0)[I_{sh0} + \mu(T - T_0)] \\ I_d = I_{d0}(T/T_0)^3 \exp\left[\frac{q}{k}\left(\frac{E_{g0}}{T_0} - \frac{E_g}{T}\right)\right] \\ E_g/E_{g0} = 1 - 0.0002677(T - T_0) \\ R_{sh} = (S_0/S)R_{sh0} \end{cases} \tag{12}$$

where E_g is the band-gap energy of PV cell, $E_{g0} = 1.121$ eV used for the diode silicon layer at STC (Dobos, 2012), and μ is the temperature coefficient of short circuit current, $\mu = 1.6 \times 10^{-4}$ A/K. The solar radiation spectrum depends on the path which a solar radiation travels through the atmosphere. Therefore, performance of a PV cell/module is related to that optical path. The air mass coefficient is defined by the direct optical path length through the Earth's atmosphere over the path length vertically upwards at the zenith. The coefficient depends on the solar radiation incident angle to the normal to the Earth's surface, i.e. solar zenith angle. At the STC, the air mass coefficient is referred to AM1.5G at 48.2° solar zenith angle. AM1.5G represents the overall yearly average for mid-latitudes. The air mass effect is excluded from the scaling laws, concerning a daily change in the solar radiation.

The six parameters of the single PV cell, shown in Table 3 at STC, are adopted and the objective function presented with Eq. (6) is optimised by using the TRR algorithm to determine the maximum electrical power under each variable climate condition. The physics models in the transient simulations include the sunlight beam reflective and refractive laws and radiation transport equation, heat conduction equation and laminar 3D Navier-Stokes equations, and their details can be found in ANSYS (2014). The materials of the CPC and solar cell, namely the top glass cover, two encapsulant layers, silicon layer and back glass cover as well as the air trapped in the cavity of the CPC are regarded as a grey and participating medium. The optical, radiative and thermal properties of those materials are independent to temperature and tabulated in Table 7.

The heat conduction equation in the two glass covers and three layers of the sylgrad and solar cell and the unsteady 3D Navier-Stokes equations inside the cavity of the CPC are solved by making use of a finite volume method. The solar radiation intensity, S, ambient temperature, T_a, and wind speed, v, in the outside condition were monitored in Ortiz-Rivera and Feliciano-Cruz (2009) with the clock time, t. To facilitate the reading by ANSYS CFX, these data are fitted by using a least squares method, and the following correlations are obtained:

$$\begin{cases} S = -0.0999t^5 + 5.753t^4 - 130.26t^3 + 1414.9t^2 - 7097.2t + 13104 \\ T_a = -4.1007 \times 10^{-4}t^5 + 2.2118 \times 10^{-2}t^4 - 0.44954t^3 \\ \quad +4.0336t^2 - 12.704t + 295.93 \\ v = -1.5554 \times 10^{-4}t^5 + 4.0814 \times 10^{-3}t^4 + 4.6919 \times 10^{-2}t^3 \\ \quad -2.4398t^2 + 25.722t - 80.733 \end{cases} \tag{13}$$

A comparison is also made in Fig. 7 between the monitored data and the estimates with Eq. (14) where a satisfactory agreement is received. A higher wind speed gives rise to an increased forced

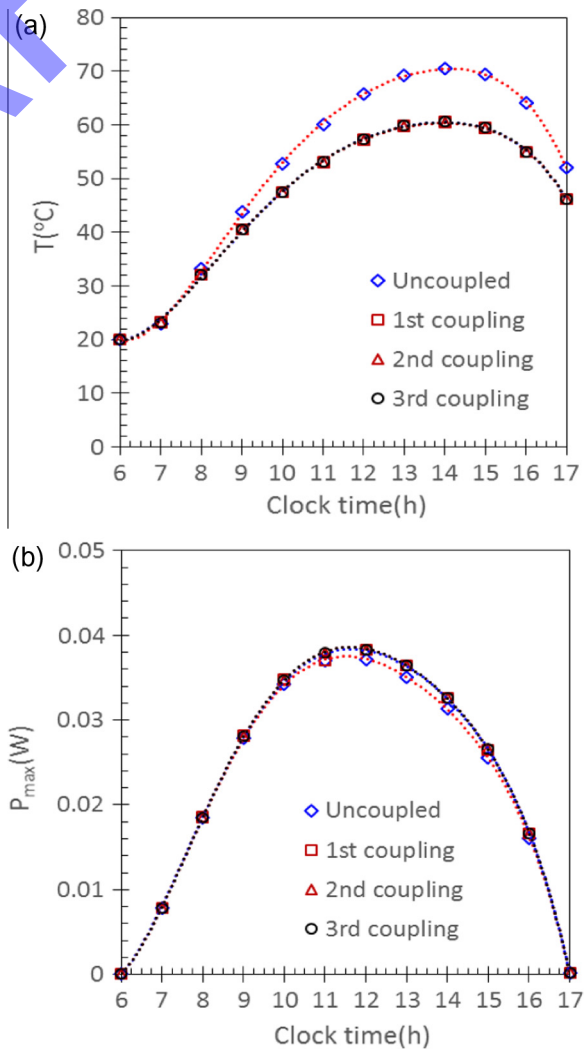

Fig. 8. Cell temperature and maximum electrical power under variable radiation intensity, ambient temperature and wind speed of a day at various iteration numbers of coupling, (a) cell temperature, (b) maximum power.

convection heat transfer coefficient over the outside surfaces of the CPC and solar cell. Based on a known wind speed, the forced heat transfer coefficient is determined by means of the Duffie correlation (Duffie and Beckman, 2013)

$$h = 5.7 + 3.8v \quad (14)$$

All the outside boundary surfaces are subject to a constant emissivity with variable air temperature and heat transfer coefficient described by Eqs. (13) and (14). The variable radiation intensity in Eq. (13) is imposed on the top glass cover under the 0° incidence by considering the CPC controlled by a tracking system. The initial velocity in the air cavity of CPC is set to zero, and a uniform temperature of 293.15 K is used as the initial temperature field; the initial radiation field is established with the Stefan-Boltzmann equation for back body at 293.15 K. A transient simulation is started at 06:00 and finished at 17:00 with a constant trade-off time step of 7.5 min.

Monte Carlo method is applied to solve the sunlight propagation into the participating media: air, glass, sylgard, silicon with a total of 200,000 number of histories under 64 target coarsening rate and 20,000 number of small coarse grid size. During the simulation process, the thermal and radiation energy equations are coupled and the fluid flow governing equations are solved for each of the 30 iterations (Li et al., 2015a). Moreover, a mesh dependency study on the simulated results suggests that the mesh size with 105,660 nodes and 82,309 hexahedral elements is sufficient enough to resolve the transportation fields and thus used in the simulations. Using a finer mesh with 176,054 nodes and 147,372 elements, it was found that the average temperature on the bottom surface of the CCPC and the back glass cover increased by only 1.2% and 0.5% respectively.

The PV cell temperature and maximum electrical power predicted under the variable solar radiation intensity and ambient temperature, as well as wind speed prescribed by Eq. (13) are illustrated in Fig. 8 in terms of the clock time at three couplings between the six-parameter electrical model in MATLAB and the CFD multiphysics simulation in ANSYS CFX. Both the cell temperature and maximum power show a significant change in the 1st coupling compared with those without the thermal and electrical coupling. Once the CFD and electrical model are coupled, the convergence of the temperature and power is very quick, suggesting that the three couplings are adequate.

While comparing with the uncoupled case, the converged coupling case exhibits a more uniform temperature profile on the top glass cover, whilst the profiles on the remaining surfaces remain the same as those in the coupling case, see Fig. 9. The air flow patterns are found to be quite similar in both the cases, but with a higher magnitude of the air velocity in the uncoupled case than that in the coupled case, because the cell temperature in the former is about 10 °C above the latter one.

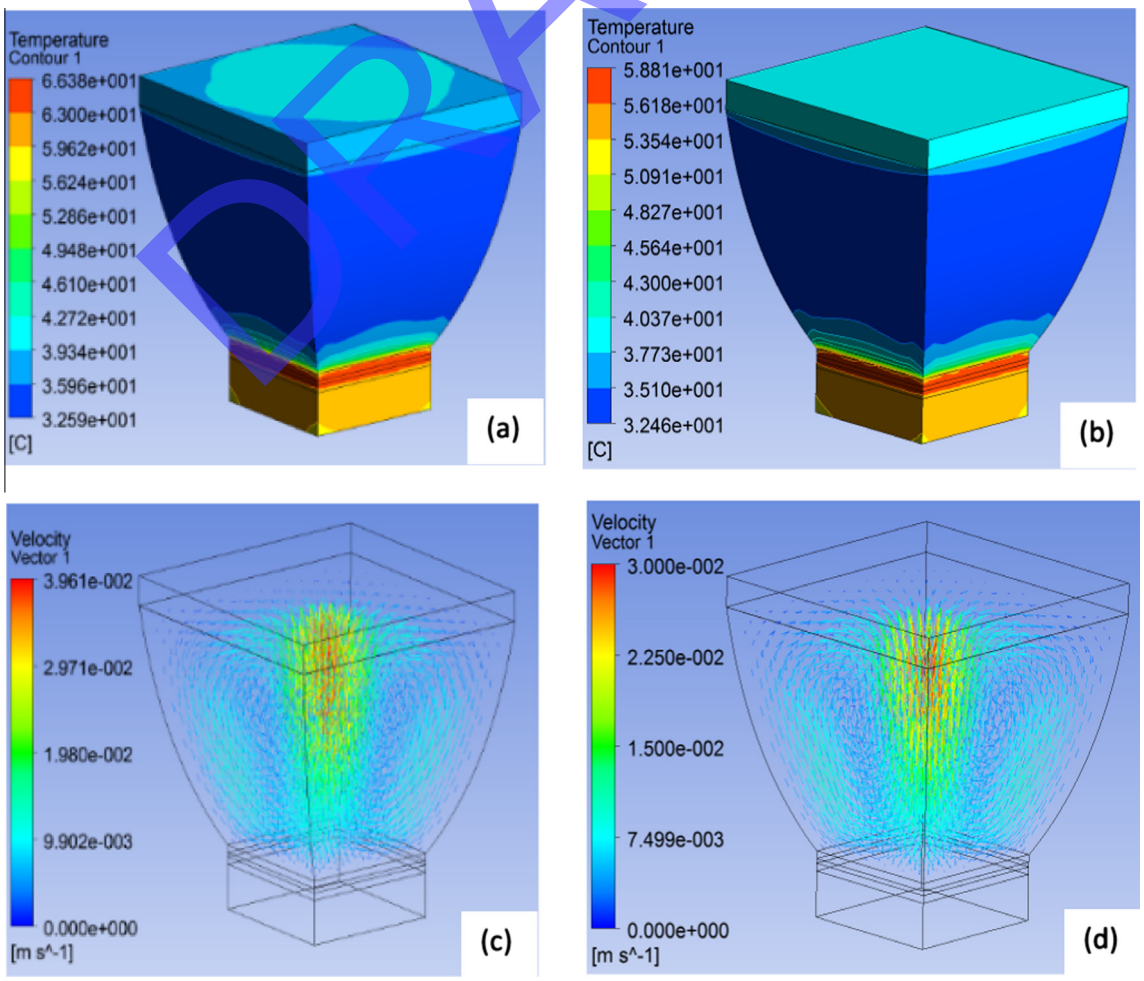

Fig. 9. Temperature profile over the CPC and PV cell surfaces and air flow pattern in the CPC cavity at 12 pm in the uncoupled and converged couple cases, (a) temperature profile, uncoupled case, (b) temperature profile, converged coupled case, (c) velocity pattern, uncoupled case, (d) velocity pattern, converged coupled case.

4. Conclusions

A lumped electrical model for the PV cells/modules with CPC is put forward by involving the CPC gain coefficient into an existing five-parameter lumped electrical model for flat-plate PV cell/module. One CPC with a single PV cell and two CPC modules with PV 2×2 and 9×9 cells are built and their I-V curves are tracked in an indoor laboratory at STC. The model is validated and fitted into the transient performance prediction of a PV cell with CPC under variable outdoor climate conditions with an aid of the scaling laws for PV cells/modules/panels.

It is shown that the optimisation algorithm used for extracting the six model parameters is more feasible and accurate compared with the existing algorithms for the five-parameter model for PV cells/modules without CPC. The ideality factor, short-circuit current and reverse saturation current are the most dominated parameter, whereas the shunt resistance is the least important, and the series resistance and CPC gain coefficient are in between.

Finally, the six-parameter model is successfully integrated with the transient multiphysics simulations in ANSYS CFX and MATLAB and the coupled optical–thermal-electrical performance of CPC with PV cell under outdoor climate conditions is investigated. The convergence of coupling is so rapid that the three-time couplings are sufficient. Additionally, two proposals are made to determine a reasonable range of the shunt resistance.

Conflict of interest

None.

Acknowledgment

The authors gratefully acknowledge the financial support received from the EPSRC through a Solar Challenge project, SUNTRAP (EP/K022156/1).

References

AlHajri, M.F., El-Naggar, K.M., AlRashidi, M.R., Al-Othman, A.K., 2012. Optimal extraction of solar cell parameters using pattern search. Renew. Energy 44, 238–245.
AlRashidi, M.R., AlHajri, M.F., El-Naggar, K.M., Al-Othman, A.K., 2011. A new estimation approach for determining the I-V characteristics of solar cells. Sol. Energy 85, 1543–1550.
ANSYS, 2014. ANSYS CFX-Solver Theory Guide, ANSYS CFX Release 15.0. ANSYS, Inc., Canonsburg, PA 15317, USA.
Askarzadeh, A., Rezazadeh, A., 2013. Extracting of maximum power point in solar cells using bird mating optimizer-based parameters identification approach. Sol. Energy 90, 123–133.
Baig, H., Sarmah, N., Chemisana, D., Rosell, J., Mallick, T.K., 2014. Enhancing performance of a linear dielectric based concentrating photovoltaic system using a reflective film along the edge. Energy 73, 177–191.
Baig, H., Sarmah, N., Heasman, K.C., Mallick, T.K., 2013. Numerical modelling and experimental validation of a low concentrating photovoltaic system. Sol. Energy Mater. Sol. Cells 113, 201–219.
Baig, H., Sellami, N., Mallick, T.K., 2015. Performance modeling and testing of a building integrated concentrating photovoltaic (BICPV) system. Sol. Energy Mater. Sol. Cells 134, 29–44.
Boyd, M.T., Klein, S.A., Reindl, D.T., Dougherty, B.P., 2011. Evaluation and validation of equivalent circuit photovoltaic solar cell performance models. ASME J. Solar Energy Eng. 133, 021005-1–021005-13.
Carrero, C., Ramirez, D., Rodriguez, J., Platero, C.A., 2011. Accurate and fast convergence method for parameter estimation of PV generators based on three main points of the I-V curves. Renew. Energy 36, 2972–2977.
Carrero, C., Rodriguez, J., Ramirez, D., Platero, C., 2010. Simple estimation of PV modules loss resistances for low error modelling. Renew. Energy 35, 1103–1108.
Chan, D.S.H., Phillips, J.R., Phang, J.C.H., 1986. A comparative study of extraction methods for solar cell model parameters. Solid-State Electron. 29 (3), 329–337.
Cooper, T., Dahler, F., Ambrosetti, G., Pedretti, A., Steinfeld, A., 2013. Performance of compound parabolic concentrators with polygonal apertures. Sol. Energy 95, 308–318.
De Soto, W., Klein, S.A., Beckman, W.A., 2006. Improvement and validation of a model for photovoltaic array performance. Sol. Energy 80, 78–88.
Ding, K., Zhang, J.W., Bian, X.G., Xu, J.W., 2014. A simplified model for photovoltaic modules based on improved translation equations. Sol. Energy 101, 40–52.
Dobos, A.P., 2012. An improved coefficient calculator for the California Energy Commission 6 parameter photovoltaic model. ASME J. Solar Energy Eng. 134, 021011-1–021011-6.
Duffie, J.A., Beckman, W.A., 2013. Solar Engineering of Thermal Processes, fourth ed. John & Sons, Inc., Hoboken, New Jersey, USA.
Easwarakhanthan, T., Bottin, J., Bouhouch, I., Boutrit, C., 1986. Nonlinear minimization algorithm for determining the solar cell parameters with microcomputers. Int. J. Solar Energy 4, 1–12.
El-Naggar, K.M., AlRashidi, M.R., AlHajri, M.F., Al-Othman, A.K., 2012. Simulated annealing algorithm for photovoltaic parameters identification. Sol. Energy 86, 266–274.
Han, W., Wang, H.H., Chen, L., 2014. Parameters identification for photovoltaic module based on an improved artificial fish swarm algorithm. Sci. World J. http://dx.doi.org/10.1155/2014/859239.
Ikegami, T., Maezono, T., Nakanishi, F., Yamagata, Y., Ebihara, K., 2001. Estimation of equivalent circuit parameters of PV module and its application to optimal operation of PV system. Sol. Energy Mater. Sol. Cells 67, 389–395.
Ismail, M.S., Moghavvemi, M., Mahlia, T.M.I., 2013. Characterization of PV panel and global optimisation of its model parameters using genetic algorithm. Energy Convers. Manage. 73, 10–25.
Kim, W., Choi, W., 2010. Estimation of equivalent circuit parameters of PV module and its application to optimal operation of PV system. Sol. Energy 84, 1008–1019.
King, D.L., Boyson, W.E., Kratochvil, J.A., 2004. Photovoltaic Array Performance Model, Sandia Report No. SAND2004-3535, Photovoltaic System R&D Department, Sandia National Laboratories, Albuquerque, New Mexico, USA.
Li, W.G., Paul, M.C., Sellami, N., 2015a. Coupled simulation of performance of a crossed compound parabolic concentrator with solar cell. Energy Proc. 75, 325–330.
Li, W.G., Paul, M.C., Sellami, N., Mallick, T.K., Knox, A.R., 2015b. Unsteady optical and thermal behaviour of crossed compound parabolic concentrator with solar cell. In: 11th Photovoltaic Science Application and Technology (PVSAT-11), Leeds, 15–17 April, UK.
Lo Brano, V., Ciulla, G., 2013. An efficient analytical approach for obtaining a five parameters model of photovoltaic modules using only reference data. Appl. Energy 111, 894–903.
Lo Brano, V., Orioli, A., Ciulla, G., 2012. On the experimental validation of an improved five-parameter model for silicon photovoltaic modules. Sol. Energy Mater. Sol. Cells 105, 27–39.
Lo Brano, V., Orioli, A., Ciulla, G., Di Gangi, A., 2010. An improved five-parameter model for photovoltaic modules. Sol. Energy Mater. Sol. Cells 94, 1358–1370.
Ma, T., Yang, H.X., Lu, X., 2014. Development of a model to simulate the performance characteristics of crystalline silicon photovoltaic modules/strings/arrays. Sol. Energy 100, 31–41.
Mammo, E.D., Sellami, N., Mallick, T.K., 2013. Performance analysis of reflective 3D crossed compound parabolic concentrating photovoltaic system for building faced integration. Prog. Photovoltaics Res. Appl. 21, 1095–1103.
MATLAB, 2015. Optimization ToolboxTM-User's Guide. The MathWorks Inc., MA 01760-2098, USA.
Orioli, A., Di Gangi, A., 2013. A procedure to calculate the five-parameter model of crystalline silicon photovoltaic modules on the basis of the tabular performance data. Appl. Energy 102, 1160–1177.
Ortiz-Rivera, E.I., Feliciano-Cruz, L.I., 2009. Performance evaluation and simulation of a solar thermal power plant. In: IEEE Energy Conversion Congress and Exposition, ECCE 2009, 20–24 September, San Jose, CA, USA.
Polverini, D., Tzamalis, G., Mullejans, H., 2011. A validated study of photovoltaic module series resistance determination under various operating conditions according to IEC 60891. Prog. Photovoltaics Res. Appl. 20, 650–660.
Rabl, A., 1976. Optical and thermal properties of compound parabolic concentrators. Sol. Energy 18, 497–511.
Sarmah, N., Natarajan, S.K., Richards, B.S., 2010. Design and Performance Valuation of a Prototype Dielectric Photovoltaic Concentrator. PVSAT-6, Southampton, UK.
Sellami, N., Mallick, T.K., 2013. Optical efficiency study of PV crossed compound parabolic concentrator. Appl. Energy 102, 868–876.
Siddiqui, M.U., Abido, M., 2013. Parameter estimation for five-and seven-parameter photovoltaic electrical models using evolutionary algorithm. Appl. Soft Comput. 13, 4608–4621.
Siddiqui, M.U., Arif, A.F.M., Kelly, L., Dubowsky, S., 2012. Three-dimensional thermal modelling of a photovoltaic module under varying condition. Sol. Energy 86, 2620–2631.
Sweet, T., Prest, M.J., Gao, M., 2015. Scalable solar thermoelectrics and photovoltaics (SUNTRAP). In: ASME-ATI-UIT 2015 Conference on Thermal Energy Systems: Production, Storage, Utilization and the Environment, 17–20 May, Napoli, Italy.
Tsuno, Y., Hishikawa, Y., Kurokawa, K., 2009. Modelling of the I-V curves of the PV modules using linear interpolation/extrapolation. Sol. Energy Mater. Sol. Cells 93, 1070–1073.
Villava, M.G., Gazoli, J.R., Filho, E.R., 2009. Comprehensive approach to modelling and simulation of photovoltaic arrays. IEEE Trans. Power Electron. 24 (5), 1198–1208.

Zagrouba, M., Sellami, A., Bouaicha, M., Ksouri, M., 2010. Identification of PV solar cells and modules parameters using the genetic algorithms: application to maximum power extraction. Sol. Energy 84, 860–866.
Zhu, X.G., Fu, Z.H., Long, X.M., Li, X., 2011. Sensitivity analysis and more accurate solution of photovoltaic solar cell parameters. Sol. Energy 85, 393–403.
Winston, R., 1974. Principles of solar concentrators of a novel design. Sol. Energy 16, 89–95.
Wolf, P., Benda, V., 2013. Identification of PV solar cells and modules parameters by combining statistical and analytical methods. Sol. Energy Mater. Sol. Cells 93, 151–157.